The Astrophysical Journal, 718:832–840, 2010 August 1 doi:10.1088/0004-637X/718/2/832

THE EFFECT OF H_2O ON ICE PHOTOCHEMISTRY

Karin I. Öberg[1,5,6], Ewine F. van Dishoeck[2,7], Harold Linnartz[3], and Stefan Andersson[4,8,9,10]
[1] Harvard-Smithsonian Center for Astrophysics, MS 42, 60 Garden St, Cambridge, MA 02138, USA
[2] Leiden Observatory, Leiden University, P.O. Box 9513, NL-2300 RA Leiden, The Netherlands
[3] Sackler Laboratory for Astrophysics, Leiden Observatory, Leiden University, P.O. Box 9513, NL-2300 RA Leiden, The Netherlands
[4] SINTEF Materials and Chemistry, P.O. Box 4760, NO-7465 Trondheim, Norway
Received 2010 April 2; accepted 2010 May 31; published 2010 July 7

ABSTRACT

UV irradiation of simple ices is proposed to efficiently produce complex organic species during star formation and planet formation. Through a series of laboratory experiments, we investigate the effects of the H_2O concentration, the dominant ice constituent in space, on the photochemistry of more volatile species, especially CH_4, in ice mixtures. In the experiments, thin (∼40 ML) ice mixtures, kept at 20–60 K, are irradiated under ultra-high vacuum conditions with a broadband UV hydrogen discharge lamp. Photodestruction cross sections of volatile species (CH_4 and NH_3) and production efficiencies of new species (C_2H_6, C_2H_4, CO, H_2CO, CH_3OH, CH_3CHO, and CH_3CH_2OH) in water-containing ice mixtures are determined using reflection-absorption infrared spectroscopy during irradiation and during a subsequent slow warm-up. The four major effects of increasing the H_2O concentration are: (1) an increase of the destruction efficiency of the volatile mixture constituent by up to an order of magnitude due to a reduction of back reactions following photodissociation, (2) a shift to products rich in oxygen, e.g., CH_3OH and H_2CO, (3) trapping of up to a factor of 5 more of the formed radicals in the ice, and (4) a disproportional increase in the diffusion barrier for the OH radical compared with the CH_3 and HCO radicals. The radical diffusion temperature dependencies are consistent with calculated H_2O-radical bond strengths. All the listed effects are potentially important for the production of complex organics in H_2O-rich icy grain mantles around protostars and should thus be taken into account when modeling ice chemistry.

Key words: astrochemistry – circumstellar matter – ISM: molecules – methods: laboratory – molecular data – molecular processes

Online-only material: color figures

1. INTRODUCTION

Observations of complex molecules toward star-forming regions and in comets demonstrate the existence of efficient pre-biotic formation mechanisms (e.g., Belloche et al. 2009; Crovisier et al. 2004). Photochemistry in icy grain mantles was suggested as a path to chemical complexity more than three decades ago (Greenberg & Hong 1974). Despite this history and a recent surge in interest, most mechanisms that produce complex molecules during UV and ion irradiation of simple ices remain poorly understood. The photochemistry has been quantified for some pure ices (Gerakines et al. 1996; Öberg et al. 2009a). In astrophysical settings, the chemistry is complicated by the observation that most ices are mixed. Predicting the outcome of ice irradiation in space thus requires a quantitative understanding of how different mixture constituents affect the ice photochemistry. Because of its prominence and its known effects on the ice binding environment, this study focuses on the effect of H_2O ice during UV irradiation of binary ice mixtures. These mixtures are not proposed to perfectly mimic the multi-component ice mixtures found in space but are used to probe the fundamental principles of ice photochemistry, principles that can then be applied to more complicated ice systems through a combination of modeling and further experiments.

Ices are common during star formation, with H_2O ice reaching abundances of 10^{-4} with respect to H_2 (e.g., Boogert et al. 2008). Simple ices—H_2O, CO, CO_2, NH_3, CH_4, and CH_3OH—form in molecular cloud (cores) through direct freeze-out and through hydrogenation and oxygenation of atoms—O, C and N—and of unsaturated molecules such as CO on grain surfaces (Tielens & Hagen 1982; Watanabe & Kouchi 2002; Ioppolo et al. 2008). From observed ice spectral features and ice maps (Bergin et al. 2002; Pontoppidan et al. 2003; Pontoppidan 2006), the formation of ices is sequential, starting with H_2O and CO_2 (and probably CH_4 and NH_3 as well). Deeper into the cloud core or later during the core contraction CO freezes out catastrophically, resulting in a second ice phase dominated by CO and later CH_3OH. The photochemistry of CH_3OH:CO ice mixtures, investigated in Öberg et al. (2009a), and of CH_4, NH_3, and CO_2 in H_2O ice mixtures are then prime targets for laboratory experiments.

Irradiation of CH_3OH and CH_3OH:CO ices result in the formation of most complex C,H,O-bearing species, such as $HCOOCH_3$, CH_3CHO, and C_2H_5OH, found in protostellar hot cores (Öberg et al. 2009a). The same molecules may also form from irradiation of CH_4:H_2O ice mixtures, however, and the relative contribution from the two ice phases to the observed complex molecule abundances is unknown. Understanding the chemistry in the H_2O-rich ice is furthermore required to predict the formation rates of the pre-biotically important N-bearing

[5] Also at Sackler Laboratory for Astrophysics, Leiden Observatory, Leiden University, P.O. Box 9513, NL-2300 RA Leiden, The Netherlands.
[6] Hubble fellow.
[7] Also at Max-Planck Institute für Extraterrestrische Physik, Giessenbachstr. 1, D-85748 Garching, Germany.
[8] Also at Department of Chemistry, Physical Chemistry, University of Gothenburg, SE-41296 Gothenburg, Sweden.
[9] Also at Leiden Observatory, Leiden University, P.O. Box 9513, NL-2300 RA Leiden, The Netherlands.
[10] Also at Gorlaeus Laboratories, Leiden Institute of Chemistry, Leiden University, P.O. Box 9502, 2300 RA Leiden, The Netherlands.

complex molecules, since the main source of N in the ice, NH_3/NH_4^+, probably forms mixed with H_2O (Bottinelli et al. 2010).

The response of ice mixtures to irradiation also governs the amount of, e.g., CH_4 that remains for thermal desorption close to the protostar. Thermal desorption of CH_4 ice is thought to result in a complex warm-carbon-chain-chemistry around some protostars (Sakai et al. 2008). One of the aims here is to investigate how the CH_4 ice photodestruction rate depends on H_2O-ice concentration and ice temperature.

Irradiation of H_2O-rich ices was first investigated in the 1960s and 1970s (e.g., Hagen et al. 1979). Since then there has been a handful of studies that have included the effects of H_2O on the overall photochemistry and two dedicated studies on the effect of different H_2O concentrations on the CH_4 chemistry during proton bombardment at 10 K (Moore & Hudson 1998) and on the CH_3OH UV photochemistry at 3 K (Krim et al. 2009). Moore & Hudson (1998) found an increasing production of CH_3OH, CH_3CHO, and CH_3CH_2OH and a decreasing production of C_2H_6 with H_2O concentration in H_2O:CH_4 mixtures. Krim et al. (2009) found an almost constant CH_3OH conversion into CO, CO_2, and H_2CO for a pure and an H_2O:CH_3OH 1:1 ice, but a factor of 3–7 conversion increase in an H_2O:CH_3OH 10:1 mixture. In both studies, all changes were explained by the production of increasing amounts of OH radicals with H_2O concentration and subsequent radical–radical reactions or H-abstraction by OH.

H_2O may however affect the photochemistry in more ways than increasing the number count of OH radicals in the ice. The binding energies in H_2O-rich ices are typically different compared with pure ices (Collings et al. 2003), which may affect radical diffusion. Radicals may also become physically trapped in H_2O ice at low temperatures as is often observed for volatile molecules (Collings et al. 2004). These radical-H_2O interactions have probably different strengths for different radicals, which may drive the chemistry in otherwise unexpected directions.

We investigate the relative importances of these potential effects of H_2O on the photochemistry of CH_4, NH_3, and CO_2 ices. The focus is on quantitative comparisons between pure and binary H_2O:CH_4 ices at different concentrations and temperatures, both during irradiation and during the subsequent warm-up.

2. EXPERIMENTS

The experiments are carried out on the set-up CRYOPAD (Öberg et al. 2005) under ultra-high vacuum conditions ($\sim 10^{-9}$–10^{-10} mbar). Ices are deposited diffusively at 18 K by introducing a gas (mixture) in the vacuum chamber along the surface normal of a gold substrate, which is temperature controlled down to 18 K with a 2 K uncertainty. 10–20 mbar gas mixtures are prepared in a separate glass manifold with a base pressure of 10^{-4} mbar. The CH_4, NH_3, and $^{13}CO_2$ ($^{13}CO_2$ was used to minimize overlap with gas-phase CO_2 features from outside of the vacuum chamber) gases have a minimum purity of 99.9% (Indugas). Samples containing H_2O are prepared from the vapor pressure of deionized H_2O, further purified through freeze thawing.

The original ice mixture as well as changes in the ice composition induced by UV irradiation are quantified through infrared spectroscopy in reflection-absorption mode (RAIRS). The relative RAIRS band strengths are consistent with relative transmission band strengths in the investigated ice thickness regime and thus certain within 20%–30% (Öberg et al. 2009c).

Table 1
The Photochemistry Experiments

Ice	H_2O:x	Temp. (K)	Thick. (ML)	Cross Section (10^{-18} cm^2)
CH_4	0:1	30	47	0.5[0.3]
H_2O:CH_4	1:3	20	42	2.8[1.4]
H_2O:CH_4	2:1	20	37	2.9[1.5]
H_2O:CH_4	4:1	20	37(29:8)	4.9[2.5]
H_2O:CH_4	4:1	40	38(30:8)	4.6[2.3]
H_2O:CH_4	5:1	60	38(32:6)	3.9[2.0]
NH_3	0:1	30	51	1.4[0.7]
H_2O:NH_3	1:1	20	54	1.5[0.8]
H_2O:NH_3	4:1	20	43	5.0[2.5]
CO_2	0:1	30	15	···
H_2O:CO_2	6:1	20	35	···

Absolute band strengths have a 50% uncertainty, but this does not affect the quantification of the chemistry, where yields are calculated in fractions of the original ice.

The ices are irradiated by a hydrogen-discharge UV lamp, peaking at Lyα but extending between 6 and 11.5 eV (Muñoz Caro & Schutte 2003). All ices are irradiated with a UV flux of $\sim 1.1(\pm 0.5) \times 10^{13}$ s^{-1} cm^{-2} for 6 hr, resulting in a total fluence of $\sim 2.3 \times 10^{17}$ cm^{-2}. This is comparable to the fluence an ice in a cloud core is exposed to during 10^6 years because of cosmic-ray-induced UV photons at a flux of 10^4 cm^{-2} s^{-1} (Shen et al. 2004). The lamp calibration is described in Öberg et al. (2009c).

Table 1 lists the photochemistry experiments in terms of their mixture composition, ice temperature during UV irradiation, and total thickness. Following irradiation at 20–100 K, all experiments are heated by 1 K minute^{-1} to 150–250 K, while acquiring RAIRS every 10 minutes. The ice thicknesses range between $\sim$15 and 54 monolayers (ML), but most experiments are carried out with $\sim$40 ML ices. These ice thicknesses are similar to what is expected in the dense and cold stages of star formation and they are also in the linear regime for RAIRS. The ices are also thick enough that photodesorption will not significantly affect the bulk of the ice, based on previously measured UV photodesorption yields (Öberg et al. 2009c, 2009b).

3. RESULTS

The following five subsections focus on (1) the photodestruction cross sections of CH_4, NH_3, and CO_2, (2) the identification of the photoproducts, (3) the H_2O:CH_4 photochemistry as a function of H_2O concentration during irradiation and (4) during warm-up, and (5) the effects of temperature on the H_2O:CH_4 UV photochemistry in dilute mixtures.

3.1. Photodestruction Cross Sections in Pure and Mixed Ices

The photodestruction rate of a species determines the production rate of radicals in the ice. Its maximum value is the photodissociation rate, as measured in the gas phase. Previous ice experiments have however shown that the measured ice photodestruction rates are substantially lower than the gas-phase photodissociation rates (Cottin et al. 2003), probably because of fast back reactions between the dissociation fragments. Figure 1 shows the $^{13}CO_2$, CH_4, and NH_3 spectral features before and after a UV fluence of 2.3×10^{17} cm^{-2} in pure ices and H_2O:X $\sim$ 5:1 ice mixtures at 20–30 K. During irradiation, more CH_4 and NH_3 are destroyed in the mixtures than in the pure ices.

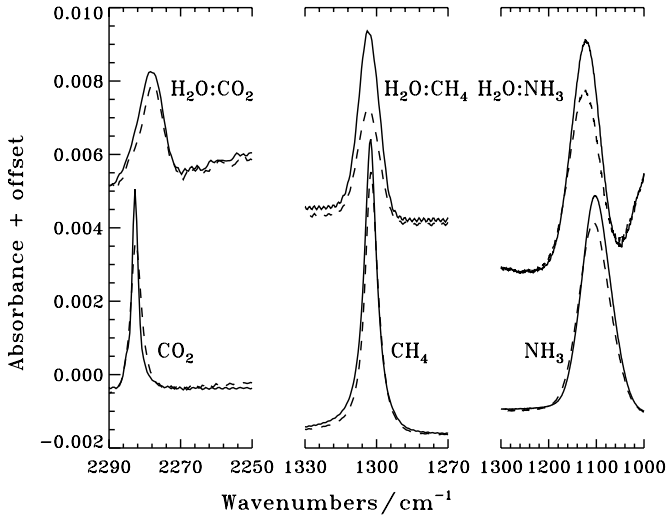

Figure 1. A $^{13}CO_2$, a CH_4, and an NH_3 ice spectral feature before (solid) and after (dashed) a UV fluence of 2.3×10^{17} cm^{-2} at 20–30 K for pure ices (bottom panel) and for H_2O:X ∼ 5:1 ice mixtures (top panel).

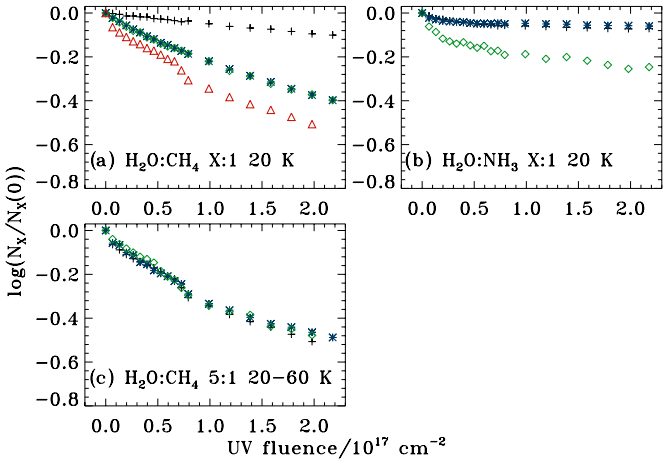

Figure 2. Normalized and log-transformed loss of CH_4 and NH_3 in (a) H_2O:CH_4 ice mixtures at 20–30 K (crosses: pure ice; stars: 1:3; diamonds: 2:1; triangles: 4:1), (b) H_2O:NH_3 ice mixtures at 20–30 K (crosses: pure ice; stars: 2:1; diamonds: 5:1), and (c) H_2O:CH_4 5:1 ice mixtures at 20–60 K (crosses: 20 K; stars: 40 K; diamonds: 60 K).

(A color version of this figure is available in the online journal.)

This effect is shown quantitatively in Figure 2, where the loss of CH_4 and NH_3 in the different ices is plotted as a function of UV fluence (overlap with gas-phase CO_2 lines prevents a similar analysis for CO_2 ice). The photodestruction cross sections are calculated from the first 4×10^{16} photons cm^{-2}, where the curves are still approximately linear, and the results are listed in Table 1—the listed uncertainties are absolute and the fit uncertainties are 10%–20%. The photodestruction cross sections for pure CH_4 and NH_3 are 0.5 and 1.4×10^{-18} cm^2, respectively. Both are an order of magnitude lower than the measured gas-phase photodissociation cross sections (van Dishoeck 1988). They are still higher than previously reported values for 1000 ML ices (Cottin et al. 2003), suggesting that those experiments may have suffered from optical depth effects.

The photodestruction cross sections are up to an order of magnitude higher in the H_2O ice mixtures, close to the gas-phase photodissociation values. In the case of CH_4, even the small amount of H_2O in the H_2O:CH_4 1:3 ice mixture results in a factor of 5 higher destruction cross section, while an H_2O-dominated ice (5:1) is required to increase the NH_3 cross section significantly.

The increasing UV photodestruction with H_2O concentration suggests that H_2O molecules surrounding the photodissociated volatiles may trap some of the radicals and thus inhibit reformation of CH_4 and NH_3. The reason behind the differences between different species is difficult to assess without further modeling, but the effect seems larger, the lighter volatile dissociation radicals (CH_3+H versus NH_2+H versus CO+O), assuming that the lack of an effect of H_2O on the final CO_2 dissociation fraction corresponds to a constant CO_2 photodissociation cross section with H_2O concentration.

Temperature does not affect the CH_4 photodestruction cross section between 20 and 60 K for dilute (∼5:1) H_2O:CH_4 ice mixtures (Figure 2(c)). The effect on more CH_4-rich ice mixtures cannot be tested because of thermal outgassing of CH_4 above 30 K when in high concentrations. In comparison, recent experiments on pure CH_3OH ice photodissociation resulted in an increasing photodestruction (then termed "effective photodissociation") cross section with temperature by up to 50% (Öberg et al. 2009a). In the CH_3OH study, this was explained by an increased escape probability of the dissociation fragments at higher temperatures, thus lowering the back-reaction rate. A similar effect was expected for CH_4. Its absence suggests that thermal diffusion is fast already at 20 K for the volatile CH_4 dissociation fragments compared with the main CH_3OH photodissociation product, CH_2OH.

3.2. Product Identification

Quantification of the ice photochemistry requires secure identifications of the main reaction products. This was not possible for the UV-irradiated H_2O:NH_3 and H_2O:CO_2 ices, because the spectral features of expected main products—NH_2OH, HCOOH, and H_2CO_3—are blended with bands of H_2O, NH_3, or other photoproducts. The expected photoproducts in H_2O:CH_4 ices are shown in Figure 3. Figure 4 shows that most of the spectral features appearing upon irradiation of H_2O:CH_4 ice mixtures can be assigned to the predicted main products: C_2H_6, H_2CO, CO (not shown), CH_3OH, CH_3CH_2OH, and CH_3CHO, in agreement with Moore & Hudson (1998). A few bands remain unassigned and are probably due to more complex molecules and to radicals. The figure also shows that two of the products, CH_3OH and CH_3CH_2OH, have bands that shift significantly between the pure ice and the H_2O mixture. This introduces some uncertainty in the assignment of CH_3CH_2OH—it is only possible to securely separate the relative contributions of CH_3OH and CH_3CH_2OH in a subset of the experiments.

In general, the spectral bands used for identification and quantitative analysis have minimum overlap with spectral features of other detected species as well as of more complex molecules (Öberg et al. 2009a). These band positions and strengths are listed in Table 2. When deriving ice abundances, the region of the investigated bands is typically fitted with several Gaussians to account for band overlaps. This approach was chosen instead of fitting ice spectra because of the varying spectral shapes in different ice environments. The same band strengths were adopted for all ice mixtures, since the exact band strengths are unknown for most of the used ice mixtures.

3.3. H_2O Concentration Effects at 20 K

Figure 5 shows that irradiation of pure CH_4 ice results in the production of C_2H_6, C_2H_4, and larger hydrocarbons, as

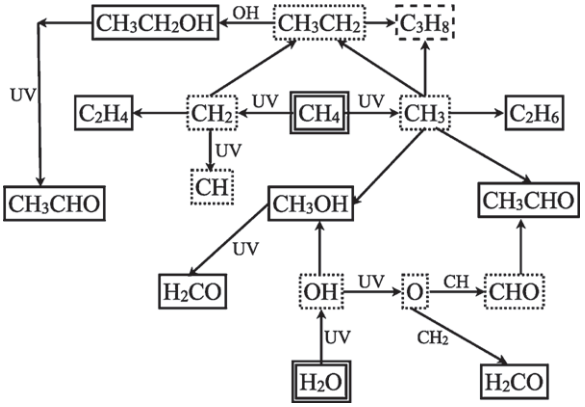

Figure 3. Reaction scheme of expected main reaction pathways during UV irradiation of H_2O:CH_4 ice mixtures. In addition, small abundances of the CH_3OH photoproducts shown in Öberg et al. (2009a) may form. Solid boxes mark species securely identified in the experiments.

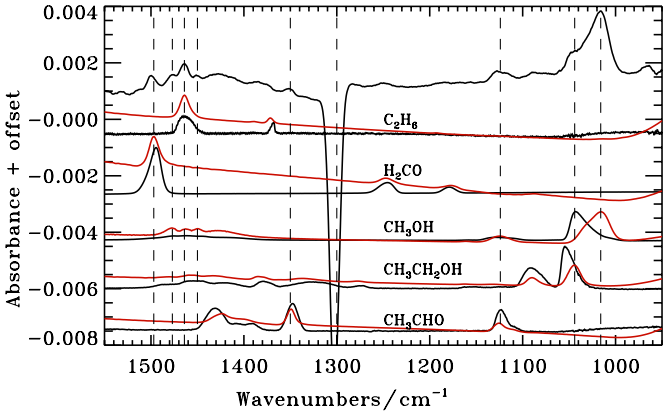

Figure 4. Spectrum of an irradiated H_2O:CH_4 2:1 mixture at 20 K is plotted on top together with pure (black) and H_2O mixtures (red) of expected products. The H_2O mixture spectra are taken from the NASA Goddard Cosmic ice laboratory spectral database by Moore et al. (http://www-691.gsfc.nasa.gov/cosmic.ice.lab).

(A color version of this figure is available in the online journal.)

expected—no C_2H_2 was observed and in general the products are hydrogen rich. Adding H_2O to the CH_4 ice results in the appearance of CO, H_2CO, CH_3OH, CH_3CHO and CH_3CH_2OH spectral features. The same bands are visible in all H_2O ice mixtures, but the relative contributions of different bands change with concentration.

The effect of H_2O concentration on the final product abundances, with respect to CH_4, is quantified in Figure 6. The identified products can be sorted into three groups: (1) hydrocarbons which have increasing abundances with CH_4 concentration, (2) small organics like CH_3OH that form from a CH_4 and an H_2O fragment, and (3) larger organics like CH_3CH_2OH that form from two CH_4 fragments and one H_2O fragment. The molecules in each group are then expected to form as

$$\frac{N_{C_2H_6}}{N_{CH_4}} \propto [CH_4], \quad (1)$$

$$\frac{N_{CH_3OH}}{N_{CH_4}} \propto (100 - [CH_4]), \text{ and} \quad (2)$$

$$\frac{N_{CH_3CH_2OH}}{N_{CH_4}} \propto (100 - [CH_4])[CH_4]. \quad (3)$$

Qualitatively, the abundance patterns of these three molecules agree with the curve predictions. The difference in, e.g., the peak position of the curve in Figure 6(c) indicates that the effects of diffusion and different photodestruction cross sections for different mixtures cannot be neglected when making quantified predictions, however. In addition, the production dependencies of H_2CO, CO, and CH_3CHO are expected to be complicated by multiple formation pathways, all involving multiple dissociation events as shown in Figure 3.

Four of the detected photoproducts, C_2H_6, CH_3OH, H_2CO, and CO, form abundantly enough to quantify their production as a function of fluence during UV irradiation (Figure 7). C_2H_6 and CH_3OH form immediately upon irradiation in all experiments. The H_2CO production is delayed in the H_2O-dominated mixture and CO production does not begin before 5×10^{16} photons cm^{-2} in any mixture as expected for a reaction pathway through multiple photodissociation events.

The initial photoproduction rates of C_2H_6, CH_3OH, and H_2CO are calculated from the abundance growth during the first 4×10^{16} photons cm^{-2} when the growth is still roughly linear. Table 3 lists the resulting formation "cross sections." These numbers do not represent physical photoproduction cross sections,

Table 2
Ice Infrared Spectral Features Used for Quantification

Species	Band (cm^{-1})	Band Strength[a] (cm^{-1})	Reference
CH_4	1300	6.1×10^{-18}	Moore & Hudson (1998)
NH_3	1070	1.7×10^{-17}	D'Hendecourt & Allamandola (1986)
CO_2	2343	7.6×10^{-17}	Gerakines et al. (1995)
H_2O	1670	1.2×10^{-17}	Gerakines et al. (1995)
C_2H_6	2976	1.1×10^{-17}	Moore & Hudson (1998)[b]
	821	1.9×10^{-18}	Pearl et al. (1991)
C_2H_4	1436	2.9×10^{-18}	Moore & Hudson (1998)[b]
H_2CO	1500	3.9×10^{-18}	Schutte et al. (1993)
CH_3OH	1026	2.8×10^{-17}	D'Hendecourt & Allamandola (1986)
CH_3CH_2OH	1044	7.3×10^{-18}	Moore & Hudson (1998)[b]
CH_3CHO	1350	6.1×10^{-18}	Moore & Hudson (1998)[b]
CO	2139	1.1×10^{-17}	Gerakines et al. (1995)

Notes.
[a] The band strengths are known within ~20%–30% when comparing results from different references, ice mixtures, and ice temperatures.
[b] In an H_2O ice matrix.

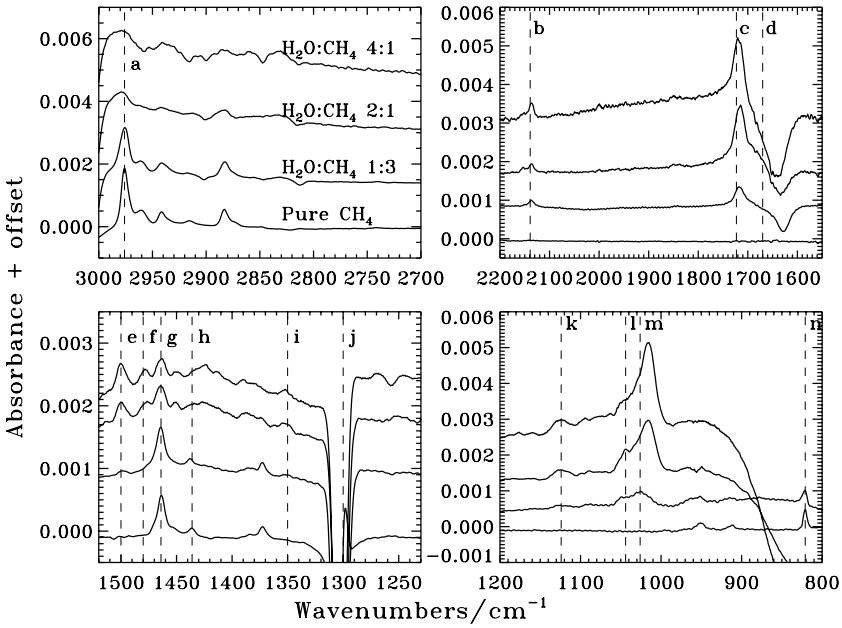

Figure 5. Difference spectra of CH_4 ice and H_2O:CH_4 ice mixtures after a UV fluence of 2.3×10^{17} photons cm^{-2}. The marked peaks are: (a) C_2H_6, (b) CO, (c) XCHO, (d) H_2O, (e) H_2CO, (f) CH_3OH, (g) C_2H_6, (h) C_2H_4, (i) CH_3CHO, (j) CH_4, (k) CH_3OH, (l) CH_3CH_2OH, (m) CH_3OH, and (n) C_2H_4.

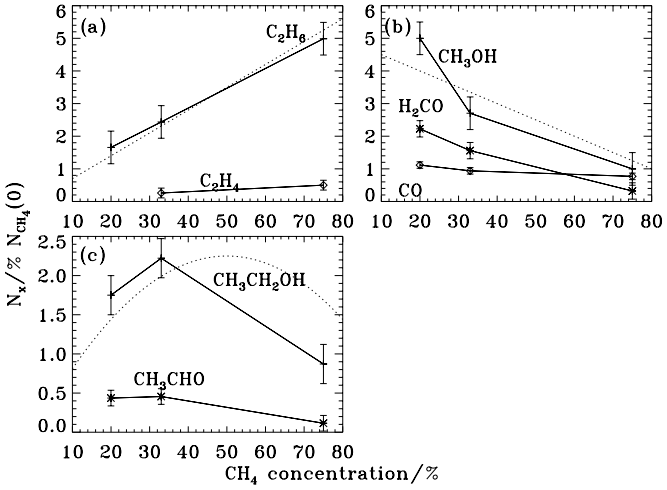

Figure 6. Normalized, final abundances of the identified photoproducts as a function of CH_4 concentration in the ice. The error bars only include the relative uncertainties and the absolute uncertainties are about a factor of 2. The dotted lines are the qualitative predictions using Equations (1)–(3).

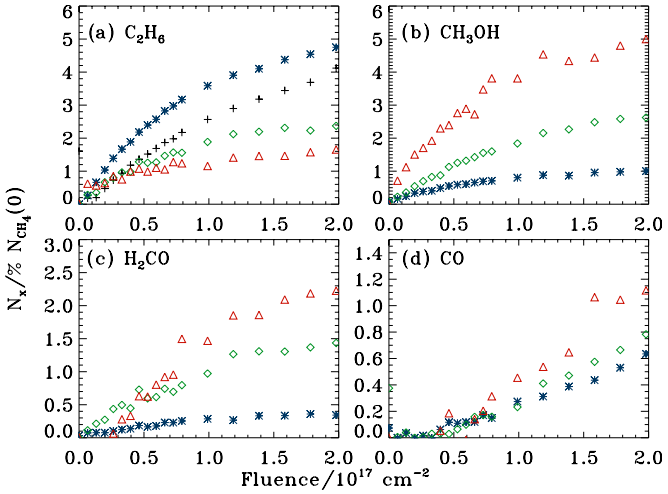

Figure 7. Quantified production of C_2H_6, CH_3OH, H_2CO, and CO in the different mixtures (crosses: pure CH_4; blue stars: H_2O:CH_4 1:3; green diamonds: 2:1; red triangles: 4:1) as a function of UV fluence.

(A color version of this figure is available in the online journal.)

since diffusion is required for their formation; it is, however, a convenient way of parameterizing their formation. The total formation cross section of complex molecules, in number of product molecules with respect to CH_4, increases somewhat with H_2O concentration. When taking into account that some products require multiple CH_x fragments, an approximately constant fraction of the original CH_4 is incorporated into more complex molecules at all concentrations. Furthermore, the CH_4 photodestruction cross section increases with an order of magnitude, between pure CH_4 and the 4:1 mixture, and the formation efficiencies normalized to the photodestruction cross sections thus *decrease* significantly with H_2O concentration. The presence of H_2O then slows down the chemistry of the radicals in the ice, even though this effect is "compensated for" under laboratory timescales by the even more efficient slow down of back reactions into CH_4.

Table 3
Normalized Product "Cross Sections" (10^{-18} $cm^2/N_{CH_4}(0)$) at 20 K for H_2O:CH_4 Ices

Product	Pure CH_4	1:3	2:1	4:1
C_2H_6	0.30[0.10]	0.52[0.18]	0.29[0.10]	$\lesssim$0.20
C_2H_4	0.04[0.01]	...	...	...
CH_3OH	...	0.11[0.04]	0.23[0.08]	0.56[0.19]
H_2CO	...	<0.02	0.15[0.05]	0.10[0.04]
Total[a]	0.34	0.63	0.67	$\lesssim$0.86
Total (%)[b]	~100	41	33	$\lesssim$22

Notes. Fit uncertainties are in brackets.
[a] The total formation cross section of new molecules.
[b] % of the photodestruction cross section that is accounted for by the total formation cross section taking into account that some molecules require multiple CH_x fragments to form.

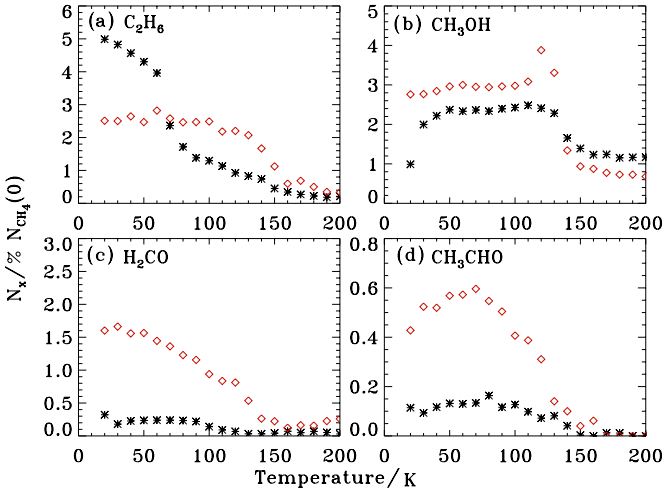

Figure 8. Quantified production and destruction of C_2H_6, CH_3OH, H_2CO, and CH_3CHO in two of the mixtures (stars: H_2O:CH_4 1:3; diamonds: 2:1) as a function of temperature during warm-up of ices irradiated at 20 K.

(A color version of this figure is available in the online journal.)

3.4. Warm-up of Irradiated Ices

During warm-up of the UV-irradiated ices, formation of new species together with sequential desorption change the ice mixture with temperature (Figure 8). In the H_2O-poor 1:3 mixture CH_3OH is the only molecule that forms perceptively during warm-up, in the 2:1 mixture CH_3CHO is alone to form until reformation of the H_2O-ice network around 130 K. The different formation patterns in the H_2O-poor and H_2O-rich ices suggest different diffusion environments. Specifically, OH diffusion seems hindered in the H_2O-rich ice, while HCO can still diffuse and react with CH_3 to form CH_3CHO. All species are partially trapped in the H_2O ice, so that even C_2H_6 desorption is only complete around the H_2O desorption temperature of ∼150 K

3.5. Ice Temperature Effects During Irradiation at 20–60 K

Increasing the ice temperature should speed up the thermal diffusion of radicals in the ice and thus the ice chemistry. Figure 9 shows that the most notable changes in the irradiated ice spectra at 20, 40, and 60 K are instead due to outgassing or a decreased production of volatile species, such as H_2CO and CO, at the higher temperatures. The decreased production of these secondary and tertiary dissociation products can be understood if the intermediate radicals, e.g., HCO diffuse fast enough at higher temperatures to react with another radical before absorbing a second photon and dissociating to CO. This scenario is supported by an earlier onset in the CH_3CHO production at 60 K compared to 20 K (Figure 10) and also consistent with the warm-up results that reveal HCO diffusion above 30 K.

In contrast, there is no evidence for an increased formation efficiency of CH_3OH and CH_3CH_2OH or for the formation of more complex molecules such as $(CH_2OH)_2$. Rather, the CH_3OH production cross section decreases from 5.6 to 3.3 × 10^{-18} $cm^2/N_{CH_4}(0)$ between 20 and 60 K. The lack of a positive temperature effect on the CH_3OH production, illustrated in Figure 10, suggests that CH_3OH and CH_3CH_2OH formation depends mainly on CH_3 diffusion that is efficient already at 20 K; OH and CH_2OH diffusion must be too slow, even at 60 K, in an H_2O-dominated ice to affect their formation. In addition, the decreasing cross section with temperature is probably due to thermal desorption of some of the produced CH_3 at 60 K before it has time to react.

4. CALCULATIONS OF BINDING ENERGIES

To aid the interpretation of the experiments, we calculated the binding energies of radical-H_2O complexes using the CCSD(T) (coupled cluster with single, double, and perturbative triple excitations) method with the aug-cc-pVTZ basis set (Kendall et al. 1992). In order to correct for the Basis Set Superposition Error, the Boys–Bernardi counterpoise method (Boys &

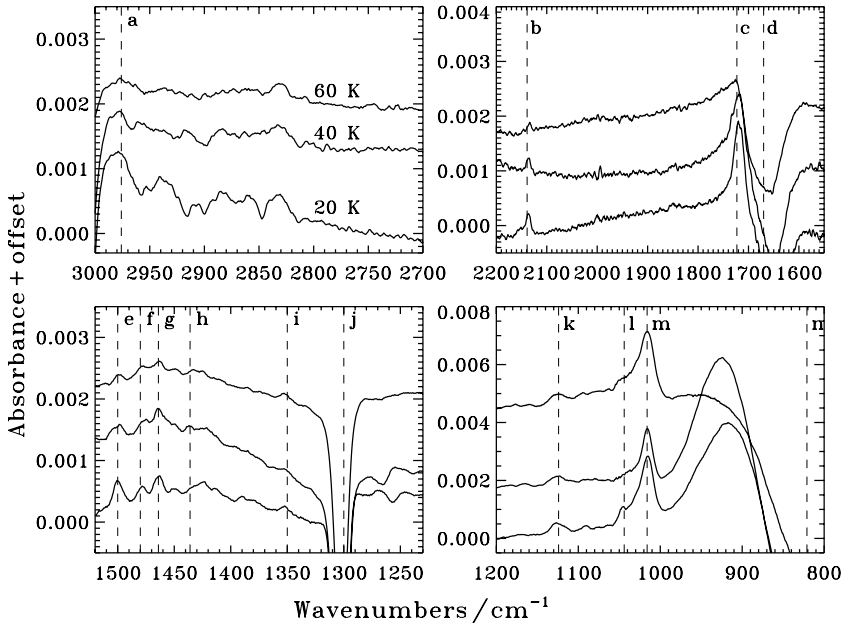

Figure 9. Difference spectra of irradiated H_2O:CH_4 4–6:1 ice mixtures at 20–60 K after a UV fluence of 2.3 × 10^{17} photons cm^{-2}. The marked peaks are identified with (a) C_2H_6, (b) CO, (c) XCHO, (d) H_2O, (e) H_2CO, (f) CH_3OH, (g) C_2H_6, (h) C_2H_4, (i) CH_3CHO, (j) CH_4, (k) CH_3OH, (l) CH_3CH_2OH, (m) CH_3OH, and (n) C_2H_4.

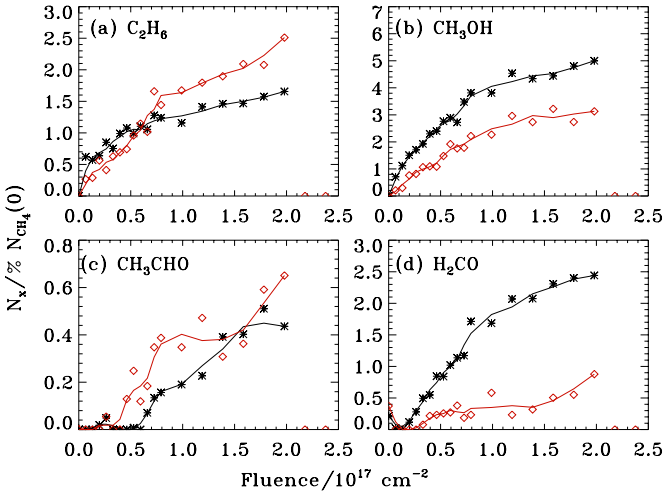

Figure 10. Quantified production of C_2H_6, CH_3OH, CH_3CHO, H_2CO, and CH_3CH_2OH in H_2O:CH_4 4–6:1 mixtures at 20 K (stars) and 60 K (red diamonds) as a function of UV fluence. The lines show the 2–3 data point averages.

(A color version of this figure is available in the online journal.)

Bernardi 1970) was used. The internal geometries of the interacting species were kept constant while a large number of different relative orientations and intermolecular distances were scanned. The thus located lowest energy minima were used to calculate the binding energies. The reported energies are electronic energies relative to the infinitely separated interaction partners. No account of zero-point energy was made. All calculations were performed using the Gaussian 03 program package (Frisch et al. 2004).

The calculations were carried out for the predicted three most common radicals in the ice, OH, HCO, and CH_3. The resulting binding energies are: 0.23 eV (2700 K) for H_2O–OH, 0.11 eV (1300 K) for H_2O–HCO, and 0.07 eV (800 K) for H_2O–CH_3. The H_2O–OH result is in good agreement with other recent high-level calculations (Soloveichik et al. 2010)

5. DISCUSSION

5.1. The Influence of H_2O

Under laboratory conditions, the most important effect of increasing the H_2O concentration is to drive the chemistry away from C_xH_y chains and toward products with a higher and higher concentration of OH. The same effect was noted by Moore & Hudson (1998) during proton bombardment of H_2O:CH_4 ice mixtures. This can be understood from simple rate equations where the production rates of various molecules are proportional to the production rates of CH_3/CH_2 and OH in the ice, i.e., the photodestruction cross sections of CH_4 and H_2O. The absolute values of these reaction rates also depend on the diffusion rates of radicals. If the destruction and diffusion rates had been constant, the relations shown in Figure 6 could have been used to derive the relative diffusion barriers directly.

H_2O does, however, change the CH_4 photodestruction cross section. Since this increased destruction efficiency is not accompanied by an equally large increase in production efficiencies of new molecules, H_2O must slow down the overall diffusion of radicals in the ice to the point of trapping them. H is not expected to be trapped at 20 K, however, and the existence of larger radicals in the ice indicates that many of the H atoms formed during dissociation either escape from the ice or react to form H_2. A significant amount of the produced heavier radicals, especially CH_3, must also remain mobile in or on top of the ice to account for the production of any complex molecules during irradiation at 20 K in the H_2O-rich ices. Without detailed modeling, it is not possible to estimate the relative importances of surface and bulk diffusion for the chemistry. It is however unlikely that all radicals are trapped in the bulk of the ice at 20 K, since even in the most dilute mixtures ∼20% of the dissociated CH_4 molecules recombine to form more complex molecules. This corresponds to at least 8 ML of chemically active ice in a 40 ML-thick ice, and the ice would thus have to be very porous to explain all chemistry with diffusion on external and internal (in large pores) ice surfaces. It would also be strange if diffusion in H_2O ices is fundamentally different compared with diffusion in CH_3OH ices, where bulk diffusion is definitely required to explain the ice photochemistry results (Öberg et al. 2009a), considering the similar behavior of the two ices during segregation studies (Ehrenfreund et al. 1999; Bernstein et al. 2005).

Trapping of some of the radicals in the ice bulk is, however, needed to explain that up to 80% of the dissociated CH_4 is not converted into more complex molecules in the H_2O:CH_4 5:1 ices. This is consistent with the commonly observed trapping of molecules such as CO and CO_2 in H_2O-rich ices (Collings et al. 2004). It may also explain some earlier results; trapping of CH_3OH photofragments in the H_2O:CH_3OH 10:1 ice mixture in Krim et al. (2009) would prevent the radicals from reacting with each other and thus favor dissociation into smaller and smaller fragments (CH_2OH, H_2CO, HCO, CO), explaining their result of high H_2CO and CO yields in H_2O-rich ices without invoking efficient H abstraction by OH radicals.

When the ice is heated, some of the bound radicals overcome their entrapment and react to form new species. In all H_2O:CH_4 ice mixtures, the most abundant radicals are expected to be CH_3 (see below) and OH, the two major photoproducts of CH_4 and H_2O. CH_3OH is thus always expected to form more abundantly during warm-up of the irradiated ices than, e.g., CH_3CHO, consistent with the results in Figure 7 for the H_2O:CH_4 1:3 experiment. In the 2:1 mixture, almost no CH_3OH forms initially during warm-up, however. Instead a significant amount of CH_3CHO forms, followed later by CH_3OH formation during the H_2O ice reformation temperature of ∼120–130 K. An increasing H_2O concentration thus increases the OH diffusion barrier relative to the HCO diffusion barrier. This is physically reasonable since OH and H_2O are expected to bond stronger than HCO and H_2O. The importance of the relative diffusion barriers of OH and HCO to drive the chemistry demonstrates that radical–radical reactions in ice are only efficient when both radicals (i.e., CH_3+OH and CH_3+HCO) taking part in the reaction are mobile.

5.2. Toward Quantifying the H_2O:CH_4 Photochemistry

CH_4 is known to dissociate into a number of different fragments during UV photolysis in the gas phase. The dissociation cross section is wavelength dependent; e.g., almost no CH_2 is observed to form from dissociation with Lyα photons (Mordaunt et al. 1993) even though it is expected to be an important channel at lower photon energies (Slanger & Black 1982). By comparing the initial C_2H_6 and C_2H_4 formation efficiencies in pure UV-irradiated CH_4 ice, it is possible to constrain the CH_4 photodissociation branching ratio in ices irradiated with a hydrogen lamp output consisting of both Lyα photons and broadband emission.

In the pure CH_4 ice, the initial growth of both C_2H_6 and C_2H_4 is assumed to be caused by CH_3+CH_3 and CH_2+CH_2

radical reactions, ignoring second generation photodissociation products. Further assuming that the diffusion barriers of CH_3 and CH_2 are comparable, the CH_4 branching ratio can be constrained from the initial C_2H_6 and C_2H_4 production rate, which is ~9:1; Gerakines et al. (1996) find a comparable C_2H_6/C_2H_4 product ratio (8:1). Since each reaction requires two radicals, the dissociation branching ratio is inferred to be CH_3:$CH_2 \gtrsim$ 3:1. This is consistent with a chemistry driven largely by Lyα photons.

The diffusion barriers are more difficult to constrain directly from the experiment. The calculated bond strengths of 800, 1300, and 2700 K for the H_2O–CH_3, –HCO, and –OH complexes are not identical to ice diffusion barriers, but the relative values should agree with the experimental results. Indeed, the data show that OH has a higher diffusion barrier than HCO in H_2O-dominated ices (efficient thermal diffusion at 30 and 120 K, respectively) and that CH_3 must be already diffusing at 20 K to explain any complex molecule production at this temperature. The calculated bond strengths are thus a good starting point for models, where the quantified formation rates of molecules can be used to extract diffusion barriers, similarly to what is currently being done for the CH_3OH photochemistry (R. T. Garrod & K. I. Öberg 2010, in preparation). Already, both calculations and experiments suggest that the temperature window between diffusion and desorption in H_2O-dominated ices is quite small for the investigated radicals, which may explain the low production yield of complex organics during warm-up (a few % of all dissociated CH_4) observed here compared to the efficient production of complex molecules observed during warm-up of irradiated CH_3OH-ices (Öberg et al. 2009a).

The calculations also show that predicting radical diffusion barriers from the bond strengths of the parent molecule to H_2O can be quite reasonable (Garrod et al. 2008); the H_2O–H_2O, H_2O–H_2CO, and H_2O–CH_4 bond strengths are 0.2, 0.07–0.13, and 0.03 eV, respectively (e.g., Szczesniak et al. 1993; Bene 1973), which is very similar to the bond strengths calculated for the H_2O-radical complex interactions. There thus seems to be a direct dependence between the H_2O-molecule and H_2O-radical interactions.

5.3. Astrophysical Implications

As shown previously for pure and mixed CH_3OH ices, UV irradiation of H_2O:CH_4 ices readily results in the production of complex molecules and this production can be quantified. After a UV fluence corresponding to ~10^6 years in a cloud core, up to 50% of the original CH_4 and 25% of the NH_3 ice have dissociated into radicals that can react into more complex species. At low temperatures most of these radicals are trapped in the ice, i.e., only ~10% of the original CH_4 ice can be converted into complex molecules during UV irradiation at low temperatures. As the protostar turns on and heats the ice, many of the trapped radicals will become mobile, resulting in a second equally important formation step of complex molecules—this step will probably be more important in space than in the lab because of the lower heating rate in astrophysical environments. Taking a typical CH_4 ice abundance of ~4% with respect to H_2O ice and an H_2O ice abundance of ~10^{-4} with respect to H_2 toward protostars (Öberg et al. 2008), this corresponds to a potential production of complex molecules of $0.04 \times 10^{-4} \times 0.1 = 4 \times 10^{-7}$ with respect to H_2. This is high enough to contribute significantly to typical hot core abundances of complex molecules ~10^{-9}–10^{-6} (Bisschop et al. 2007).

Table 4
CH_4 Ice Lifetimes in Years

UV Flux (cm^{-2} s^{-1})	Pure CH_4	2:1	4:1
10^4 (cloud core)	6×10^6	1×10^6	6×10^5
10^8 (cloud edge)	6×10^2	1×10^2	6×10^1
10^{11} (outflow cavity)	0.6	0.1	0.06

Several of the CH_3OH and H_2O:CH_4 photochemistry products are the same, e.g., CH_3CH_2OH and CH_3CHO, and the relative importance of the two production pathways during star formation will depend on the relative abundances of CH_3OH and CH_4 ice on the grains as well as what other ice constituents are mixed with H_2O. Both the H_2O- and the CO/CH_3OH-rich ice phases must clearly be modeled to accurately predict the total formation rates of C- and O-containing complex molecules in space.

In addition, it is crucial to understand the effects of H_2O quantitatively to constrain when and where N-containing complex molecules form—their main formation pathway is probably from NH_3 in an H_2O-rich ice. While the production of radicals seems to be the most important effect of H_2O on the ice photochemistry under laboratory conditions, this is not necessarily the case for the timescales and ice compositions present at star and planet formation. Rather, detailed modeling is required that extracts the microscopic properties of the H_2O-rich ice chemistry from the laboratory experiments, such as the composition-dependent diffusion barriers, and applies these results to astrochemical models. Only when a simple system, such as H_2O:CH_4, is understood at this detailed level, can we expect to accurately model the more elusive nitrogen chemistry in H_2O-rich environments and thus provide predictions of, e.g., the prebiotic amino acid production.

Estimating ice lifetimes is easier than predicting the chemical evolution, though the composition dependence of CH_4 photodestruction introduces some uncertainty. Table 4 lists the photodestruction timescales for 20–30 K CH_4 ice in pure, 2:1 and 4:1 H_2O:CH_4 ices subject to a weak UV field induced by cosmic rays, the interstellar radiation field, and the 1000 times higher UV flux inferred toward the L1527 outflow (Spaans et al. 1995). Outside of protected cloud cores, the CH_4 ice lifetime is thus short compared to most other timescales, especially in H_2O-rich ice mixtures relevant for protostars. For large quantities of CH_4 ice to survive to thermally desorb around protostars and drive warm-carbon-chain-chemistry as suggested by Sakai et al. (2008), it requires that the ices are well protected up until that point. This may be a reason for the low number of observations of such a chemistry during the protostellar stage.

6. CONCLUSIONS

1. The photodestruction cross section of NH_3 and CH_4 in H_2O ice mixtures increases with H_2O concentration by up to a factor of 10 with implications for the CH_4 ice lifetime in protostellar envelopes. Simultaneously, the production efficiency of stable molecules in the H_2O:CH_4 ice increases by a factor of 2. This is explained by trapping of radicals in the H_2O-ice matrix, which prevents back reactions between, e.g., CH_3 and H.
2. The H_2O:CH_4 photochemistry produces C_2H_6, CH_3OH, and CH_3CH_2OH as a function of CH_4 concentration, in a way that can be directly related to the number of OH

and CH_2/CH_3 groups in each product. The production of CH_3CHO, H_2CO, and CO has a fluence delay consistent with formation through more steps compared to, e.g., CH_3OH.

3. On laboratory timescales, increasing the ice temperature from 20 to 60 K has a limited effect on the chemistry, probably because HCO is the only important reactant that becomes mobile in this temperature interval in H_2O-dominated ice mixtures.
4. The CH_4 photodissociation branching ratio of CH_3 and CH_2 is $\gtrsim$3:1, as derived from the relative production efficiencies of C_2H_6 and C_2H_4.
5. OH diffusion is fast in the H_2O:CH_4 1:3 mixture but not present in the H_2O-dominated ice mixtures below 100 K. HCO diffusion is possible above 30 K in the H_2O-rich ice mixtures and CH_3 diffusion seems efficient at 20 K in all mixtures, consistent with calculated H_2O-radical complex bond strengths. OH diffusion is thus more severely slowed down with H_2O concentration than the other radicals, which counteracts the higher OH production rate in H_2O-richer ices.
6. Because H_2O is both a source of OH radicals and preferentially trap OH compared to more volatile radicals, predicting the photoproduction branching ratio of different complex molecules in space requires microscopic modeling of the H_2O:CH_4 experiments rather than direct comparison with experiments.

This work has benefitted from discussions with Herma Cuppen and Robin Garrod. Support for K.I.O. is provided by NASA through Hubble Fellowship grant awarded by the Space Telescope Science Institute, which is operated by the Association of Universities for Research in Astronomy, Inc., for NASA. Astrochemistry in Leiden is supported by a SPINOZA grant of the Netherlands Organization for Scientific Research (NWO) and NOVA. The work by S.A. was partly funded by an NWO-CW Top grant. Some of the electronic structure calculations were performed at C3SE (Chalmers Centre for Computational Science and Engineering) computing resources.

REFERENCES

Belloche, A., et al. 2009, A&A, 499, 215
Bene, J. E. D. 1973, Chem. Phys. Lett., 23, 287
Bergin, E. A., Alves, J., Huard, T., & Lada, C. J. 2002, ApJ, 570, L101
Bernstein, M. P., Cruikshank, D. P., & Sandford, S. A. 2005, Icarus, 179, 527
Bisschop, S. E., Jørgensen, J. K., van Dishoeck, E. F., & de Wachter, E. B. M. 2007, A&A, 465, 913
Boogert, A. C. A., et al. 2008, ApJ, 678, 985
Bottinelli, S., et al. 2010, ApJ, in press
Boys, S. F., & Bernardi, F. 1970, Mol. Phys., 19, 553
Collings, M. P., Dever, J. W., Fraser, H. J., & McCoustra, M. R. S. 2003, Ap&SS, 285, 633
Collings, M. P., et al. 2004, MNRAS, 354, 1133
Cottin, H., Moore, M. H., & Bénilan, Y. 2003, ApJ, 590, 874
Crovisier, J., et al. 2004, A&A, 418, L35
D'Hendecourt, L. B., & Allamandola, L. J. 1986, A&AS, 64, 453
Ehrenfreund, P., et al. 1999, A&A, 350, 240
Frisch, M. J., et al. 2004, Gaussian 03 Program Package (Rev. E.01; Wallingford: Gaussian, Inc.)
Garrod, R. T., Weaver, S. L. W., & Herbst, E. 2008, ApJ, 682, 283
Gerakines, P. A., Schutte, W. A., & Ehrenfreund, P. 1996, A&A, 312, 289
Gerakines, P. A., Schutte, W. A., Greenberg, J. M., & van Dishoeck, E. F. 1995, A&A, 296, 810
Greenberg, J. M., & Hong, S.-S. 1974, in IAU Symp. 60, Galactic Radio Astronomy, ed. F. J. Kerr & S. C. Simonson (Cambridge: Cambridge Univ. Press), 155
Hagen, W., Allamandola, L. J., & Greenberg, J. M. 1979, Ap&SS, 65, 215
Ioppolo, S., Cuppen, H. M., Romanzin, C., van Dishoeck, E. F., & Linnartz, H. 2008, ApJ, 686, 1474
Kendall, R. A., Dunning, T. H., Jr., & Harrison, R. J. 1992, J. Chem. Phys., 96, 6796
Krim, L., Lasne, J., Laffon, C., & Parent, P. 2009, J. Phys. Chem. A, 113, 8979
Moore, M. H., & Hudson, R. L. 1998, Icarus, 135, 518
Mordaunt, D. H., et al. 1993, J. Chem. Phys., 98, 2054
Muñoz Caro, G. M., & Schutte, W. A. 2003, A&A, 412, 121
Öberg, K. I., Garrod, R. T., van Dishoeck, E. F., & Linnartz, H. 2009a, A&A, 504, 891
Öberg, K. I., Linnartz, H., Visser, R., & van Dishoeck, E. F. 2009b, ApJ, 693, 1209
Öberg, K. I., van Dishoeck, E. F., & Linnartz, H. 2009c, A&A, 496, 281
Öberg, K. I., et al. 2005, ApJ, 621, L33
Öberg, K. I., et al. 2008, ApJ, 678, 1032
Pearl, J., Ngoh, M., Ospina, M., & Khanna, R. 1991, J. Geophys. Res., 96, 17477
Pontoppidan, K. M. 2006, A&A, 453, L47
Pontoppidan, K. M., et al. 2003, A&A, 408, 981
Sakai, N., Sakai, T., Hirota, T., & Yamamoto, S. 2008, ApJ, 672, 371
Schutte, W. A., Allamandola, L. J., & Sandford, S. A. 1993, Icarus, 104, 118
Shen, C. J., Greenberg, J. M., Schutte, W. A., & van Dishoeck, E. F. 2004, A&A, 415, 203
Slanger, T. G., & Black, G. 1982, J. Chem. Phys., 77, 2432
Soloveichik, P., O'Donnell, B. A., Lester, M. I., Francisco, J. S., & McCoy, A. B. 2010, J. Phys. Chem. A, 114, 1529
Spaans, M., Hogerheijde, M. R., Mundy, L. G., & van Dishoeck, E. F. 1995, ApJ, 455, L167
Szczesniak, M. M., Chalasinski, G., Cybulski, S. M., & Cieplak, P. 1993, J. Chem. Phys., 98, 3078
Tielens, A. G. G. M., & Hagen, W. 1982, A&A, 114, 245
van Dishoeck, E. F. 1988, in Rate Coefficients in Astrochemistry, ed. T. J. Millar & D. A. Williams (Dordrecht: Kluwer), 49
Watanabe, N., & Kouchi, A. 2002, ApJ, 567, 651